pISSN 1229-3008 eISSN 2287-6251
Progress in Superconductivity and Cryogenics
Vol.20, No.4, (2018), pp.46~49
https://doi.org/10.9714/psac.2018.20.4.046

# Refinement of $Gd_2O_3$ inclusions in the $GdBa_2Cu_3O_{7-\delta}$ films fabricated by the RCE-DR process

**I. Park[a], W. J. Oh[a], J. H. Lee[b], S. H. Moon[b], and S. I. Yoo[a,*]**

[a] *Department of Materials Science & Engineering and Research Institute of Advanced Materials (RIAM), Seoul National University, Seoul, Korea*
[b] *Superconductor, Nano & Advanced Materials Corporation, Anseong, Korea*

(Received 17 December 2018; revised or reviewed 29 December 2018; accepted 30 December 2018)

**Abstract**

To improve in-field critical current densities ($J_c$) of $GdBa_2Cu_3O_{7-\delta}$ (GdBCO) coated conductors(CCs) fabricated by the reactive co-evaporation by deposition and reaction (RCE-DR) process, employing the nominal composition of Gd:Ba:Cu=1:1:2.5, we tried to refine the $Gd_2O_3$ particles trapped in the GdBCO superconducting matrix. For this purpose, we carefully selected the processing conditions on the stability phase diagram of GdBCO for this composition. By lowering the growth temperature of $Gd_2O_3$ in the liquid, we could refine the average particle size of $Gd_2O_3$ particles trapped in the GdBCO matrix and also achieve the zero-resistive transition temperatures ($T_{c,zero}$) of 92.3~94.2 K. Unfortunately, however, it was unsuccessful to achieve enhanced in-field $J_c$ values from these samples because of an air-contamination of the amorphous precursor film before its conversion into crystalline GdBCO film, suggesting that any exposure of the amorphous precursor film to air is fatal in obtaining high performance GdBCO CCs via the RCE-DR process.

*Keywords*: $GdBa_2Cu_3O_{7-\delta}$, $Gd_2O_3$ nanoparticles, RCE-DR, critical current density, stability phase diagram

## 1. INTRODUCTION

The second generation high-temperature superconductors (HTS), so-called coated conductors (CCs), are commercialized as long-length $YBa_2Cu_3O_{7-\delta}$ (YBCO) and $REBa_2Cu_3O_{7-\delta}$ (REBCO, RE: rare earth elements) superconducting wires have been successfully fabricated via various processes such as metal-organic deposition (MOD) [1], pulsed laser deposition (PLD) [2], metal-organic chemical vapor deposition (MOCVD) [3], and reactive co-evaporation by deposition and reaction (RCE-DR) [4–5] processes. However, higher performance HTS CCs under high magnetic fields are still required for the electric power applications since the critical currents ($I_c$) of YBCO and REBCO CCs are drastically decreased in high magnetic fields [6]. Thus, many research groups have tried to improve in-field $J_c$ values of CCs by doping [7–9], irradiation [10, 11], and defect [12].

While GdBCO CCs fabricated via the RCE-DR process exhibit the highest self-field $J_c$ value, in-field $J_c$ values are inferior to CCs fabricated by other processes [13] because of less effective flux pinning. According to previous reports, $Gd_2O_3$ particles are trapped in the GdBCO matrix [4], and act as a pinning center [14]. In this work, in order to improve the pinning properties of GdBCO CCs, we tried to refine the $Gd_2O_3$ particles incorporated in the GdBCO matrix by properly controlling the nucleation and growth rate of $Gd_2O_3$ in the liquid on the basis of the stability phase diagram of GdBCO recently identified by our group [15]. For this study, an amorphous precursor film with the nominal composition of Gd:Ba:Cu = 1:1:2.5 was deposited by a reactive co-evaporation with an electron gun in SuNAM, and subsequent refinement of $Gd_2O_3$ particles trapped in the GdBCO film was performed in our laboratory.

## 2. EXPERIMENTAL

The amorphous precursor films were fabricated by a RCE-DR equipment of SuNAM. For the conversion from amorphous phase to superconducting phase, the conversion process was performed using a 6-zone reel-to-reel tube furnace shown in Fig. 1, in which the oxygen partial pressure of each 3 zone can be controlled differently.

Fig. 2 shows the processing routes on the stability phase diagram of GdBCO for the nominal composition of Gd:Ba:Cu = 1:1:2.5 [15]. The conversion conditions of GdBCO were fixed at 861°C in the $PO_2$ of 150 mTorr by

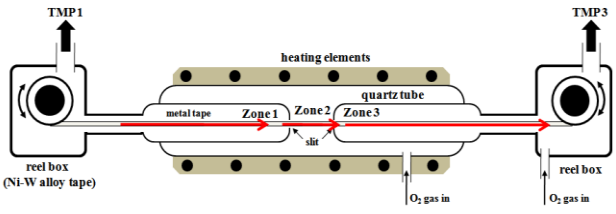


Fig. 1. The schematic of reel-to-reel tube furnace apparatus.

* Corresponding author: siyoo@snu.ac.kr

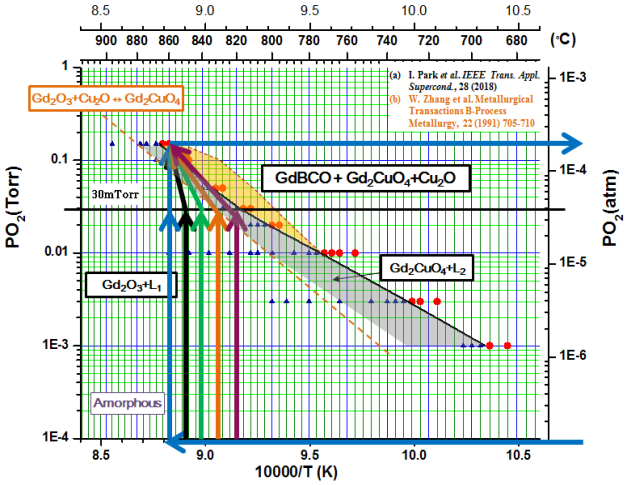


Fig. 2. The stability phase diagram of GdBCO for the nominal composition of Gd:Ba:Cu = 1:1:2.5 [15] with different fabrication process paths.

considering a undercooling temperature just below the phase boundary (866± 2°C) in the $PO_2$ of 150 mTorr. Also, the growth temperatures of $Gd_2O_3$ were varied from 821°C to 861°C and held for ~ 5 sec at the given $PO_2$ of 30 mTorr. The growth time of GdBCO films was ~ 1 min at 861°C in the $PO_2$ of 150 mTorr.

The phases of samples were analyzed by X-ray diffraction (XRD) using an X-ray diffractometer (Bruker, D8-Advance). The resistivity versus temperature ($\rho$-T) curves of samples were measured using the standard four point probe method. An analytical transmission electron microscope (TEM) (JEOL, JEM-2100F) was used to analyze the cross-sectional microstructures of samples. The TEM specimens were prepared by focused ion beam (FIB) (SII Nanotechnology, SMI 3050SE).

## 3. RESULT AND DISCUSSION

The XRD patterns of samples after oxygenation at 500°C for 1 h are shown in Fig. 3. For a comparison, the XRD pattern of the sample fabricated at the same temperature of 860°C in the $PO_2$ of 30 and 150 mTorr for the growth of $Gd_2O_3$ and GdBCO, respectively, by RCE-DR in SuNAM is also represented in Fig. 3(a). Here, it must be noted that the amorphous precursor tape prepared by reactive co-evaporation in SuNAM was exposed to air for a short term before its conversion into the superconducting phase in our lab while it was not exposed to air for the sample (a) in SuNAM. Unlike other XRD patterns including only the $Gd_2O_3$ phase, the XRD pattern of the sample (f) held at 821°C in 30 mTorr for the growth of $Gd_2O_3$ and held at 861°C in 150 mTorr for the growth of GdBCO include the $Gd_2CuO_4$ phase in addition to the $Gd_2O_3$ phase, which is marked as "5".

The $\rho$-T curves of samples are shown in Fig. 4. The $T_{c,zero}$ values of samples (a) - (f) are 93.6 K, 92.3 K, 93.3 K, 94.2 K, 94.1 K, and 93.6 K, respectively. A variation in the $T_{c,zero}$ values is not so significant, but the normal-state resistivity curves show much higher than that of the

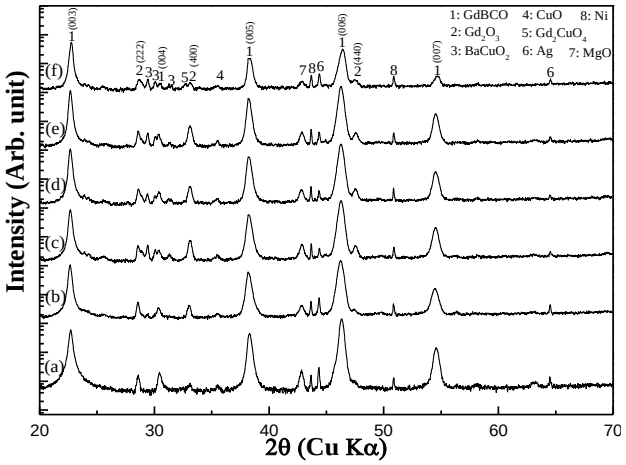


Fig. 3. The XRD patterns of the sample fabricated by RCE-DR in SuNAM (a), and the samples after growth at (b) 861°C, (c) 851°C, (d) 841°C, (e) 831°C, and (f) 821°C in 30 mTorr $O_2$ for the growth of $Gd_2O_3$ and at 861°C in the $PO_2$ of 150 mTorr for the conversion into GdBCO.

RCE-DR sample from SuNAM as shown in the inset of Fig. 4. The reason for this difference is most probably attributed to an air-exposure of the amorphous precursor films before those were set in the tube furnace for the conversion process in our lab. Further, the magnetic $J_c$-$B$ curves (though not represent here), evaluated by measuring the magnetization hysteresis curves, showed almost one order of magnitude lower than those of the RCE-DR sample (a) from SuNAM. An air-contamination might degrade the subgrain boundaries of as-grown GdBCO films into weak links resulting in higher normal-state resistivity values and also degraded in-field $J_c$ values.

However, regardless of the above disappointing result, the effect of the growth conditions of $Gd_2O_3$ on its average particle sizes could be characterized by analyzing the microstructures taken from scanning transmission electron

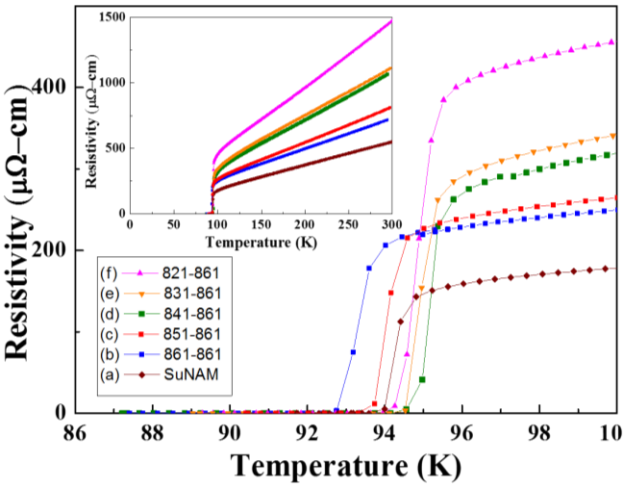


Fig. 4. The $\rho$-T curves for the GdBCO CC fabricated by RCE-DR in SuNAM (a), and also for GdBCO films grown at 861°C in 150 mTorr after the heat-treatment at (b) 861°C, (c) 851°C, (d) 841°C, (e) 831°C, and (f) 821°C in 30 mTorr for the size control of $Gd_2O_3$ particles.

microscopy (STEM)-energy dispersive X-ray spectroscopy (EDS) elemental mapping for 861-861, 841-861, and 821-861 samples, where the sample IDs denote the growth temperature of $Gd_2O_3$ in 30 mTorr - that of GdBCO in 150 mTorr. The cross-sectional TEM micrographs for these samples are represented in Fig. 5.

According to Figs. 5 (a)-(1), (2), and (3), bright round particles are $Gd_2O_3$ since Ba and Cu are free except Gd, and dark round particles are CuO or $BaCuO_2$ since Gd is free. Also, the matrix is GdBCO since all three elements of Gd, Ba, and Cu are detectable. These analysis results are exactly same with our previous report [4]. For the sample 861-861, the average particle size is 245.24 ± 50.5 nm. In the case of the sample 841-861, it can be seen that the $Gd_2O_3$ particles are relatively smaller than those in (a), and its average particle size is 128.09 ± 36.6 nm. The TEM micrograph of sample 821-861 in Fig. 5 (c) shows that the $Gd_2O_3$ particles seem to be rather bigger even though the growth temperature is lowered. However, the EDS mapping data in Figs. 5 (c)-(1), (2), and (3) show that there exist not only Gd but also Ba and Cu elements together, indicating that the bright region is not the $Gd_2O_3$ phase but the GdBCO phase.

Since the sample 821-861 in Fig. 5(c) shows a peculiar microstructure different from those of the samples 861-861 and 841-861 in Fig. 5 (a) and (b), and further a round particle (red box) in the bright region shown in Fig. 5 (c) is also observed, we performed a high resolution TEM analysis on this particle as shown in Fig. 6. In Figs. 6 (c)-(e), the bright region is GdBCO, and dark round particles must be the $Gd_2CuO_4$ phase particle since Gd and Cu are detectable but Ba is free. It is in good agreement with the XRD pattern in Fig. 3 (f) and the stability phase diagram of GdBCO in Fig 2. Since the processing routes passed the stable region of "$Gd_2CuO_4$ + L" (purple line in Fig. 2), the GdBCO phase might be formed from not only from $Gd_2O_3$ + L but also from $Gd_2CuO_4$ plus liquid, and thus $Gd_2CuO_4$ particle might be trapped in the GdBCO matrix phase. We speculate that $Gd_2CuO_4$ might react with the liquid (Ba-Cu-Oxide) phase by the peritectic recombination to form the GdBCO phase with relatively slower conversion rate compared with the peritectic recombination of $Gd_2O_3$

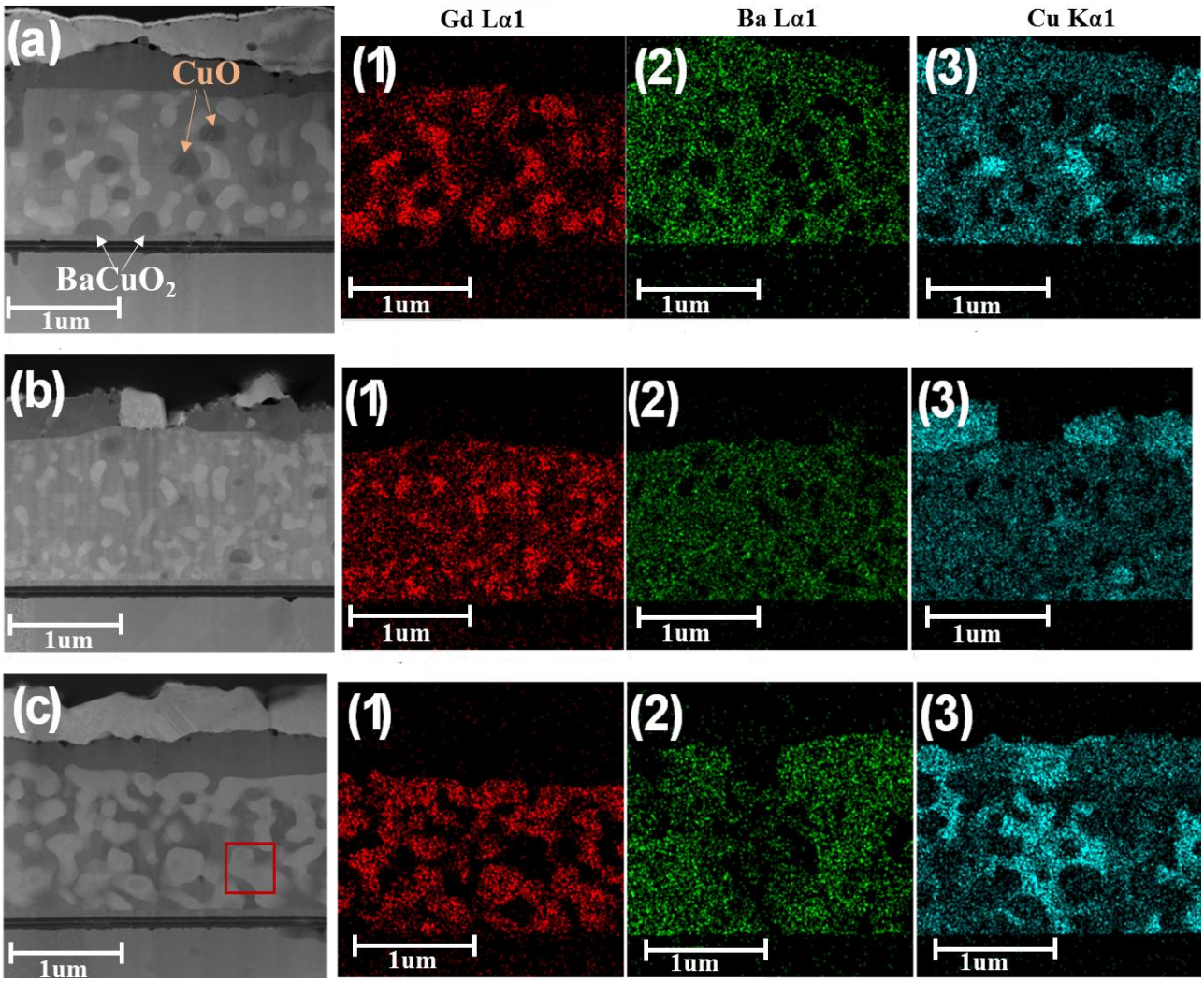


Fig. 5. Z-contrast STEM micrographs of the sample (a) 861-861, (b) 841-861, and (c) 821-861, (1) Gd, (2) Ba, and (3) Cu elements spectral images analysed for the its samples, respectively.

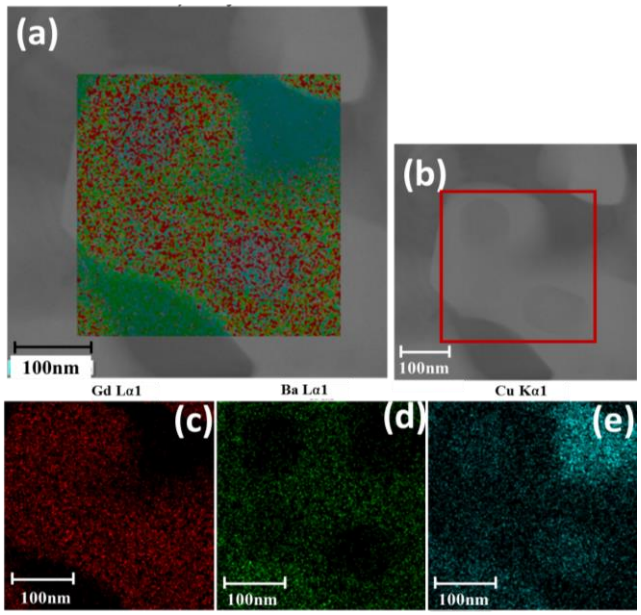


Fig. 6. Z-contrast STEM micrograph of the sample (a) and (b) 821-861, (c) Gd, (d) Ba, and (e) Cu elements spectral images analysed for the sample 821-861.

plus liquid, and hence the GdBCO matrix phase are not fully connected each other.

## 4. CONCLUSION

For the enhancement of the pinning properties, we tried to refine the $Gd_2O_3$ inclusions in the GdBCO films by controlling conversion processing conditions of the amorphous precursor film into the GdBCO film. In conclusion, although it was unsuccessful to confirm the enhancement of pinning properties due to the air-contamination by the refinement of $Gd_2O_3$ particles trapped in the GdBCO superconducting matrix, we could control their average particle size since, at relatively lower growth temperature of $Gd_2O_3$ in the liquid, more refined $Gd_2O_3$ particles were observable in the GdBCO matrix by TEM analysis. Therefore, we believe that higher in-field $J_c$ values will be achievable from the samples with more refined $Gd_2O_3$ particles if we avoid the air contamination problem of the amorphous precursor film like the normal process of RCE-DR in SuNAM since the pinning properties are expected to become more effective.

## ACKNOWLEDGMENT

This work was supported by the Korea Institute of Energy Technology Evaluation and Planning(KETEP) and the Ministry of Trade, Industry & Energy(MOTIE) of the Republic of Korea (No. 20131010501800).

## REFERENCES

[1] M. W. Rupich, X. Li, C. Thieme, S. Sathyamurthy, S. Fleshler, D. Tucker, E. Thompson, J. Schreiber, J. Lynch, D. Buczek, K. DeMoranville, J. Inch, P. Cedrone, and J. Slack, "Advances in second generation high temperature superconducting wire manufacturing and R&D at American Superconductor Corporation," *Superconductor Science and Technology*, vol. 23(1), 014015, 2010

[2] H. Kutami, T. Hayashida, S. Hanyu, C. Tashita, M. Igarashi, H. Fuju, and Y. Hanada, "Progress in research and development on long length coated conductors in Fujikura," *Physica C-Superconductivity and Its Applications*, vol. 469(15-20), pp. 1290-1293, 2009.

[3] V. Selvamanickam, Y. Chen, X. Xiong, Y. Y. Xie, M. Martchevski, A. Rar, Y. Qiao, T. M. Schmidt, A. Knoll, K. P. Lenseth, and C. S. Weber, "High Performance 2G Wires: From R&D to Pilot-Scale Manufacturing," *IEEE Transactions on Applied Superconductivity*, vol. 19(3), pp. 3225-3230, 2009.

[4] S. M. Choi, J. W. Lee, G. H. Shin, J. H. Lee, G. W. Hong, S. H. Moon, and S. I. Yoo, "Characteristics of high-Jc GdBCO coated conductors fabricated by the RCE-DR process," *IEEE Transactions on Applied Superconductivity*, vol. 23(3), 8001004, 2013.

[5] J. H. Lee, H. Lee, J. W. Lee, S. M. Choi, S. I. Yoo, and S. H. Moon, "RCE-DR, a novel process for coated conductor fabrication with high performance," *Superconductor Science and Technology*, vol. 27(4), 044018, 2014

[6] S. R. Foltyn, J. L. MacManus-Driscoll, Q. X. Jia, B. Maiorov, H. Wang, and M. Maley, "Materials science challenges for high-temperature superconducting wire," *Nat. Mater.*, vol. 6, pp. 631–642, 2007.

[7] K. Matsumoto, T. Horide, K. Osamura, M. Mukaida, Y. Yoshida, A. Ichinose, and S. Horii, "Enhancement of critical current density of YBCO films by introduction of artificial pinning centers due to the distributed nano-scaled $Y_2O_3$ islands on substrates," *Physica C*, vol. 412, pp. 1267–1271, 2004.

[8] J. L. MacManus-Driscoll, S. R. Foltyn, Q. X. Jia, H. Wang, A. Serquis, L. Civale, B. Maiorov, M. E. Hawlry, M. Maley, and D. E. Peterson, "Strongly enhanced current densities in superconducting coated conductors of $YBa_2Cu_3O_{7-x}$ + $BaZrO_3$," *Nature Mater.* vol. 3, pp. 439–443, 2004.

[9] Y. Yamada, K. Takahashi, H. Kobayashi, M. Konishi, T. Watanabe, A. Ibi. T. Muroga, S. Miyata, T. Kato, T. Hirayama, and Y. Shiohara, "Epitaxial nanostructure and defects effective for pinning in $Y(RE)Ba_2Cu_3O_{7-x}$ coated conductors," *Appl. Phys. lett.*, vol. 87, 132502, Sep. 2005.

[10] W. Schindler, B. Roas, G. Saemann-Ischenko, L. Schultz, and H. Gerstenberg, "Anisotropic enhancement of the critical current density of epitaxial $YBa_2Cu_3O_{7-x}$ films by fast neutron irradiation," *Physica C*, vol. 169, pp. 117–122, 1989.

[11] B. Roas, B. Hensel, G. Saemann-Ischenko, and L. Schultz, "Irradiation-induced enhancement of the critical current density of epitaxial $YBa_2Cu_3O_{7-x}$ thin films," *Appl. Phys. Lett*. vol. 54, pp. 1051–1053, 1989.

[12] Goyal, S. Kang, K. J. Leonard, P. M. Martin, A. A. Gapud, M. Varela, M. Parathanman, A. O. Ijaduola, E. D. Specht, J. R. Thopson, D. K. Christen, S. J. Pennycook, and F. A. list, "Irradiation-free, columnar defects comprised of self-assembled nanodots and nanorods resulting in strongly enhanced flux-pinning in $YBa_2Cu_3O_{7-\delta}$ films," *Superconductor Science and Technology*, vol. 18(11), pp.1533−1538, 2005.

[13] Senatore, C. Barth, M. Bonura, M. Kulich, and Mondonico, G, "Field and temperature scaling of the critical current density in commercial REBCO coated conductors." *Superconductor Science and Technology*, vol. 29(1), 014002, 2015.

[14] J. L. MacManus-Driscoll, M. Bianchetti, A. Kursumovic, G. Kim, W. Jo, H. Wang, J. H. Lee, G. W. Hong, and S. H. Moon, "Strong pinning in very fast grown reactive co-evaporated $GdBa_2Cu_3O_7$ coated conductors," *APL Materials*, vol. 2(8), 086103, 2014.

[15] I. Park, W. J. Oh, J. H. Lee, S. H. Moon, and S. I. Yoo, "Stability phase diagram of $GdBa_2Cu_3O_{7-d}$ for the nominal composition of Gd:Ba:Cu = 1:1:2.5 in low oxygen pressures," *IEEE Transactions on Applied Superconductivity*, vol. 28(4), 7200105, 2018